Research Square

Preprints are preliminary reports that have not undergone peer review.
They should not be considered conclusive, used to inform clinical practice,
or referenced by the media as validated information.

Rheology of High-Consistency Fiber Foams: Fiber Volume Fraction as a Key Structural Parameter

Daniel Matamoros-Arnáez
VTT Technical Research Center of Finland
Juliane Carolin Kade
VTT Technical Research Center of Finland
Olli-Ville Laukkanen
VTT Technical Research Center of Finland
Antti Koponen
antti.koponen@vtt.fi

VTT Technical Research Center of Finland

Research Article

Keywords: Cellulose fiber foams, High consistency, Rheology, Solid volume fraction, Fiber volume fraction, Viscosity, Storage modulus, Loss modulus

Posted Date: November 25th, 2026

DOI: https://doi.org/10.21203/rs.3.rs-11398834/v1

License: This work is licensed under a Creative Commons Attribution 4.0 International License.
Read Full License

Additional Declarations: No competing interests reported.

Rheology of High-Consistency Fiber Foams: Fiber Volume Fraction as a Key Structural Parameter

Daniel Matamoros-Arnáez, https://orcid.org/0009-0009-1362-7404

Juliane Carolin Kade, https://orcid.org/0000-0003-4210-3932

Olli-Ville Laukkanen, https://orcid.org/0009-0000-4507-938X

Antti Koponen https://orcid.org/0000-0002-9361-6693

VTT Technical Research Centre of Finland Ltd, P.O. Box 1603, FIN-40401 Jyväskylä, Finland

Correspondence: Antti Koponen

e-mail: antti.koponen@vtt.fi

Keywords: Cellulose fiber foams, High consistency, Rheology, Solid volume fraction, Fiber volume fraction, Viscosity, Storage modulus, Loss modulus

Abstract

This study investigates the rheological behavior of high-consistency aqueous cellulose fiber foams, with fiber consistencies of 12–18% (w/w) and air contents of 63–80%. The foams exhibit Herschel–Bulkley fluid characteristics, including a distinct yield stress and power-law behavior at high shear rates. Amplitude sweep measurements reveal a predominantly elastic response at small deformations, with the storage modulus (G') exceeding the loss modulus (G'') up to a critical strain amplitude. Furthermore, the shear stiffness of high-consistency fiber foams is dominated by the presence of a continuous, three-dimensional fiber network within the foam. A key methodological contribution is the introduction of fiber volume fraction as a unified structural parameter integrating fiber consistency and air content, enabling direct correlation between fiber foam microstructure and rheology. Within this framework, the storage modulus exhibits a power-law dependence on fiber volume fraction analogous to density-dependent scaling of stiffness in rigid fiber networks and scaling predictions from the tube model. These findings provide a foundation for understanding and optimizing the rheological behavior of high-consistency fiber foams and their processing.

Introduction

During the last fifteen years, foam forming has been studied intensively as an alternative to water forming for making both traditional and novel products from natural and man-made fibers (Hjelt *et al*. 2022; Lehmonen *et al*. 2020; Ketola *et al*. 2022a). The advantages of foam forming include high uniformity of the obtained structures, the possibility to include many types of raw materials, and the ability to make highly porous lightweight materials and layered

structures. Moreover, foam forming is generally efficient in terms of raw material, energy, and water use.

A key advantage of foam forming is based on the rheological properties of aqueous foams (Dollet *et al*. 2014). Foam forming is typically performed at an air content of 60–80%, with fiber consistency (w/w) being a few percent. (Fiber consistency is the pulp mass as a percentage of the total mixture mass.) In this region, foams can be processed like viscous fluids, and their viscosity is clearly higher than that of water. The high viscosity decreases fiber mobility, while bubble–fiber interactions reduce fiber–fiber contacts, entanglement, and reflocculation. Foams used in foam forming also exhibit a yield stress, which further decreases the mobility of fibers during the late stages of forming when the shear stress is small. These key properties help explain the improved homogeneity achieved when using foam as the transporting medium instead of water.

The rheological properties of fiber foams are a relatively new topic of research. A few studies have examined microscopic interactions that govern their behavior. For example, Ketola *et al*. (2022b) investigated bubble–fiber interactions in the presence of surfactants and how these interactions influence the structure of foam-formed materials. Li *et al*. (2025) studied the effect of fiber aspect ratio on bubble dynamics and the viscosity of bagasse suspensions with fiber consistencies below 0.6% (w/w). In addition to these microscopic-scale investigations, a few studies have examined the macroscopic rheology of fiber foams using a pipe rheometer. Jäsberg *et al*. (2015, 2017) studied the rheology of hardwood (birch) pulp fiber foams at 2.0% fiber consistency. Prakash *et al*. (2021) extended this work by varying the hardwood fiber consistency between 2% and 5%. In all these studies, the foams had an air content of 70%, and sodium dodecyl sulfate (SDS) was used as the surfactant. The foams showed shear-thinning, power-law behavior, with the consistency index rising linearly with fiber concentration. At 5% fiber consistency, the consistency index was nearly five times that of pure foam.

In industrial processes that use water to transport cellulosic fibers, such as paper and board production, drying is often one of the most energy-intensive steps. Removing large quantities of water from fiber suspensions requires substantial thermal input, making it a major driver of operating costs. As a result, the efficiency of this stage plays a critical role in overall process economics, directly affecting energy consumption, throughput, and profitability. Consequently, there is increasing pressure to develop foam-forming processes that can operate at much higher fiber consistencies, preferably above 10%. By reducing the amount of water that must be removed downstream, high-consistency foam forming offers the potential to significantly lower drying energy demands, improve resource efficiency, and enhance the overall profitability of fiber-based industrial operations. However, developing such processes requires a deeper scientific understanding of the rheology of fiber foams at these high consistencies. At present, such rheological data are largely non-existent, creating a critical knowledge gap that limits process optimization and technological advancement.

Operating with high fiber consistencies not only improves process efficiency but also opens the door to entirely new applications and fiber-based products. When the foam–fiber mixture becomes sufficiently concentrated, its pronounced viscoelastic properties may enable advanced

forming methods and the fabrication of complex, lightweight, and sustainable fiber-based materials that would be difficult to produce using fiber suspensions or low-consistency aqueous fiber foams.

Fiber foams exhibit complex rheological behavior influenced by several parameters, including fiber consistency and air content. Rather than treating these two factors separately, this study introduces the fiber volume fraction as a unified structural parameter. This metric provides a clearer basis for understanding how structural reinforcement by fibers affects the viscoelastic properties, such as the storage modulus, of high-consistency fiber foams. This work is part of a project focused on developing 3D printing of fiber foams. Here, we briefly examine the rheology of high-consistency fiber foams and propose a power-law relationship for the storage modulus of aqueous cellulose fiber foams based on the fiber volume fraction. A more comprehensive study describing the full concept and experimental results will be presented in a subsequent publication.

Materials and methods

Materials

Chemi-thermomechanical pulp (CTMP) derived from spruce was obtained from the Rottneros mill in Sweden, whereas bleached hardwood kraft pulp (BHKP) derived from birch was obtained from Metsä Group's Äänekoski mill in Finland. Both were screw pressed before use. The pulp moisture content was determined using a Sartorius MA 100 moisture analyzer, while fiber length and width were measured using an ABB Lorentzen & Wettre (LW) Fiber Tester Plus+. Dry solids content was 28% and 40% for CTMP and BHKP, respectively. The mean length-weighted fiber length and width of CTMP were 1.78 mm and 38 µm, respectively, with a fines content of 62% (ISO 16065-2; fines defined as particles < 0.2 mm), while the corresponding values for BHKP were 0.97 mm and 23 µm, respectively, with a fines content of 20%.

The coarseness of the CTMP and BHKP fibers was 127 µg/m and 157 µg/m, respectively. In most experiments, the proportion of BHKP and CTMP fibers was equal. In one trial, the BHKP proportion was 25% (w/w), and in another, 75% (w/w). All chemicals were obtained from Sigma-Aldrich. As the surfactant, a mixture of sodium dodecyl sulfate (SDS) and polysorbate 20 (Tween 20) was used.

The additives were selected based on their potential effects on both foam preparation and the properties of the final 3D-printed structures, which were the primary focus of the broader project. Methylcellulose (MC) was added as a binder and thickening agent. As a cellulose ether derivative with a degree of substitution varying from 0 to 3, it can work as a surfactant and reduce particle agglomeration with different polar (-OH) and non-polar ($-OCH_3$) groups available for weak interactions (Coughlin *et al.* 2021*;* Nasatto *et al.* 2015). Microcrystalline cellulose (MCC) was tested, as small fibers, such as nanocellulose, can facilitate the binding of longer fibers by forming bridges between them (Hafez and Tajvidi 2021). MCC was selected as a cellulose-based particulate additive with a smaller anticipated effect on mixture viscosity

than nanocellulose. Polyethylene glycol (PEG) was added to evaluate its ability to facilitate foam preparation at high consistency, where the low water content can make the mixture too viscous to foam properly. By reducing the storage modulus and thereby softening the material, PEG was considered a useful additive in this context (Miranda-Valdez *et al.* 2023).

The tap water was soft, with a water hardness of approximately 0.2–0.5 mmol/L. Aqueous solutions of Tween 20, SDS, PEG 10000, and MC were prepared at concentrations of 25%, 10%, 9%, and 3% (w/w), respectively, and added to the foam mixture. A Silverson L 5M-A mixer was used to produce the PEG and MC solutions. Microcrystalline cellulose (MCC) was added in powder form.

Fiber foam preparation

The foam mixtures were produced using a Netzsch Shearmaster mixer equipped with a specialized mixing head that introduces air into the mixture as it rotates, promoting effective foaming at high consistency. The BHKP and MCC (in the case of the samples that contained this additive) were suspended in tap water at approximately 50 °C and stirred at speeds of 250–400 rpm. If a sample contained PEG, the solution was introduced at this stage. To initiate foaming, SDS, Tween 20, and the MC solution were incorporated. After several minutes of mixing, CTMP was added, and the stirring speed was later increased to 400–600 rpm. Mixing continued until the air content, defined as the fraction of the foam volume occupied by air, reached equilibrium. The final foams had air contents ranging from 63% to 80% (see Table 1). The final air content depended on the fiber consistency, SDS and Tween 20 dosages, and MCC content. The air content was quantified from the apparent density of the wet foam by measuring the mass of foam (m_f) in the rheometer cup of known volume (V) and comparing it with the mass of water (m_w) occupying the same volume. The air content (%) was calculated as $A = (1 - m_f/m_w) \times 100$.

The trial plan is shown in Table 1. The sample codes are defined as follows: *REF* = reference without MC, *C* = fiber consistency in % (w/w), the value following "+" = MCC dosage in % (w/w), *H* = BHKP proportion in % (w/w), *A* = air content in %, *P* = PEG 10000 dosage in % (w/w).

Table 1. From left to right: sample code, fiber consistency, proportion of BHKP/CTMP fibers, dosage of SDS and Tween 20 (they were the same), MCC dosage, MC dosage, PEG dosage, the final air content of the foam, the fiber volume fraction (FVF) in the foam, and storage modulus and loss modulus in the LVE region. Sample code marked with an asterisk denotes a separate sample with the same composition and air content.

Sample code	Consistency (%)	BHKP/ CTMP (%)	SDS, Tween (g/L)	MCC (%)	MC (%)	PEG (%)	Air Content (%)	FVF (%)	G'_{LVE} (kPa)	G''_{LVE} (kPa)
REF/C12/H50/A75.3	12	50/50	0.8	0	0	0	75.3	1.97	10	1.82
REF/C12/H50/A73.5	12	50/50	0.8	0	0	0	73.5	2.11	7.61	1.44
C12+0/H50/A74.4	12	50/50	0.8	0	0.5	0	74.4	2.12	9.2	1.86
C12+0/H50/A71.4	12	50/50	0.8	0	0.5	0	71.4	2.38	10.09	2.03
C14+0/H50/A70.5	14	50/50	0.8	0	0.5	0	70.5	2.85	16.99	3.2
C14+0/H50/A74.9	14	50/50	1	0	0.5	0	74.9	2.41	13.76	2.69
C12+2/H50/A72.5	12	50/50	0.8	2	0.5	0	72.5	2.65	10.6	1.96
C16+0/H75/A75.1	16	75/25	1.6	0	0.5	0	75.1	2.73	11.59	2.13
C14+2/H50/A71.6	14	50/50	1.6	2	0.5	0	71.6	2.96	18.34	3.33
C14+2/H50/A75.1	14	50/50	1.2	2	0.5	0	75.1	2.73	12.48	2.25
C16+0/H50/A63.3	16	50/50	1.2	0	0.5	0	63.3	4.03	32.9	5.91
C16+0/H50/A64.8	16	50/50	1.6	0	0.5	0	64.8	3.86	25.89	4.76
C16+0/H50/A75.4	16	50/50	1.6	0	0.5	0	75.4	2.70	11.85	2.23
C16+0/H50/A74.5	16	50/50	1.6	0	0.5	0	74.5	2.80	15.73	2.93
C16+0/H50/A74.5*	16	50/50	1.6	0	0.5	0	74.5	2.80	15.61	2.93
C18+0/H50/A68.8	18	50/50	2.4	0	0.5	0	68.8	3.84	30.51	5.18
C18+0/H50/A76.1	18	50/50	2.4	0	0.5	0	76.1	2.94	15.76	2.94
C16+2/H50/A68.0	16	50/50	1.6	2	0.5	0	68	3.94	26.86	4.51
C16+2/H50/A71.0	16	50/50	2	2	0.5	0	71	3.56	24.81	4.22
C16+0/H25/A71.7	16	25/75	2	0	0.5	0	71.7	3.10	14.54	2.73
C12+0/H50/A71.6/P1.5	12	50/50	0.8	0	0.5	1.5	71.6	2.65	8.58	1.8
C14+0/H50/A71.7/P1.5	14	50/50	1.2	0	0.5	1.5	71.7	3.00	11.05	2.15
C16+0/H50/A67.0/P1.5	16	50/50	1.6	0	0.5	1.5	67	3.95	29.28	5.24
C16+0/H50/A80.0/P1.5	16	50/50	2	0	0.5	1.5	80	2.39	6.93	1.41
C16+0/H50/A75.6/P1.5	16	50/50	2	0	0.5	1.5	75.6	2.91	13.17	2.51
C18+0/H50/A70.2/P1.5	18	50/50	2	0	0.5	1.5	70.2	3.96	27.97	4.87

Rheological measurements

The rheological measurements were performed with a stress-controlled TA Instruments DHR-2 rheometer equipped with a wide-gap vane-in-cup geometry (see Figure 1). The temperature of the sample was maintained at 22 °C with a Peltier jacket that was connected to a Julabo AWC 100 bath. The cup with a serrated surface was 3D-printed to eliminate wall slip, following the design introduced by Carraretto *et al*. (2022). The diameter of the four-blade vane was 15 mm, and the inner diameter of the cup was 30 mm, resulting in an effective measurement gap of 7.5 mm. The vane geometry was positioned vertically in the middle of the cup, with the lower edge of the vane located 16 mm above the bottom of the cup and the upper

edge located 16 mm below the upper surface of the sample to avoid end effects. The use of such a wide-gap vane geometry further minimizes possible wall slip effects (Mohtaschemi *et al*. 2014) and avoids confinement effects that would be caused by the large size of the flocs compared to the measurement gap (Barnes *et al*. 2001). Notice that the small-gap approximation, typically applicable to standard rheometer geometries such as concentric cylinder, parallel plate or cone-and-plate setups, does not hold for the wide-gap vane-in-cup geometry. Therefore, the shear rate varies radially within the sample (Chaparian *et al*. 2022), and is, strictly speaking, an apparent shear rate; however, for simplicity, the term "shear rate" is used hereafter. All rheological data were obtained from the TRIOS software (TA Instruments) that used the so-called "Couette analogy" in the calculation of rheological properties, as described in Vadillo *et al*. (2025). Fiber foam samples were transferred to the rheometer cup using an open-cut syringe. The cup was filled from the bottom while the syringe was gradually moved upwards, thereby minimizing compression of the foam. Care was also taken to avoid the formation of air pockets. The cup was weighed at this stage to determine the air content of the sample.

The oscillatory measurements included amplitude sweep measurements (γ_0 = 0.01–200 %, ω = 10 rad/s) and frequency sweep measurements (ω = 0.316–100 rad/s, γ_0 = 0.03 %). A relatively high measurement frequency was used in the amplitude sweep measurements to shorten the measurement time, since the drying and coarsening of the foam can change its rheological properties considerably with time. The shear rate sweep measurements were performed by first increasing the shear rate from 0.01 to 100 s^{-1} and then decreasing it from 100 to 0.01 s^{-1}. At each shear rate, the material was allowed to equilibrate for 5 s before data collection. The measurement time at the lowest shear rate was 30 s and decreased with increasing shear rate using a scaled time average (scale factor 0.3). Only data obtained during the decreasing shear-rate sweep are reported here, as the data measured at increasing shear rates were observed to contain measurement artifacts possibly due to shear banding or other flow inhomogeneities.

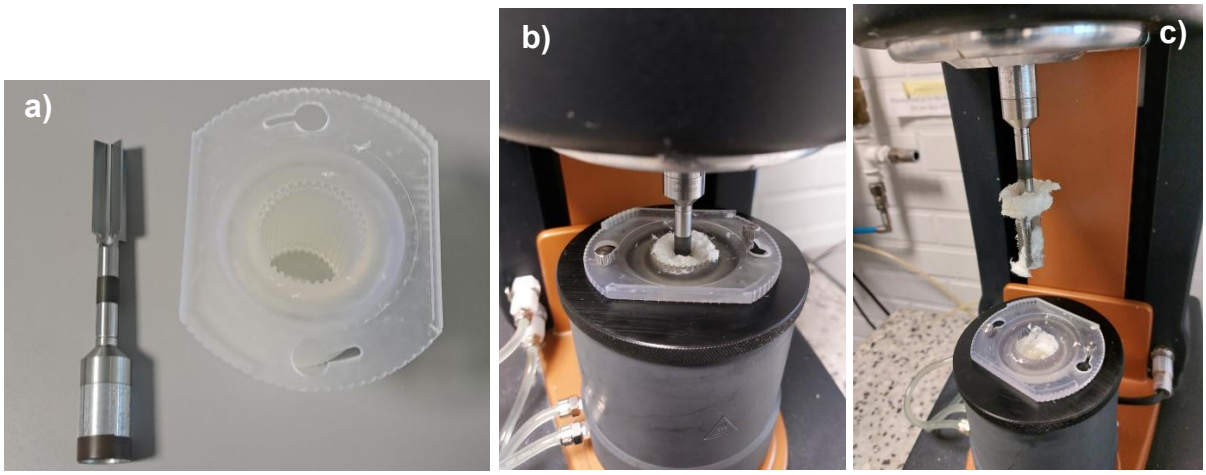

Figure 1 a) The vane geometry and the 3D-printed serrated cup used in this study. b) The measurement setup. c) The vane after removal from the sample following the measurement.

Results and discussion

Shear Rate Sweeps

Figure 2a and Figure 2b show an example of shear stress as a function of shear rate, and viscosity versus shear rate, respectively. The stress vs. shear rate curve resembles that of a typical Herschel–Bulkley fluid, namely

$$\sigma(\dot{\gamma}) = \sigma_0 + K\dot{\gamma}^n, \quad (1)$$

where σ is the shear stress, σ_0 the yield stress, K is the consistency index, and n is the flow index. The materials thus exhibit a yield stress, and their viscous behavior approximately follows a power law at high shear rates. Similar behavior was also observed for other fiber foam samples. We fitted Eq. (1) to the shear stress vs. shear rate curves, and examples of the fits are shown in Figure 2 with solid lines for a fiber foam sample with 12% consistency, a BHKP ratio of 50%, and 71.4% air content (C12+0/H50/A71.4). We see that, generally, the fit works very well. At the highest shear rates, some data points deviate from the fitted curves, which may indicate the onset of secondary flows. This could be due to the vane-in-cup geometry being more sensitive to these effects than traditional rheometer geometries, such as parallel-plate or concentric cylinder setups (Crawford *et al*. 2016). Similar behavior was observed across many fiber foam samples.

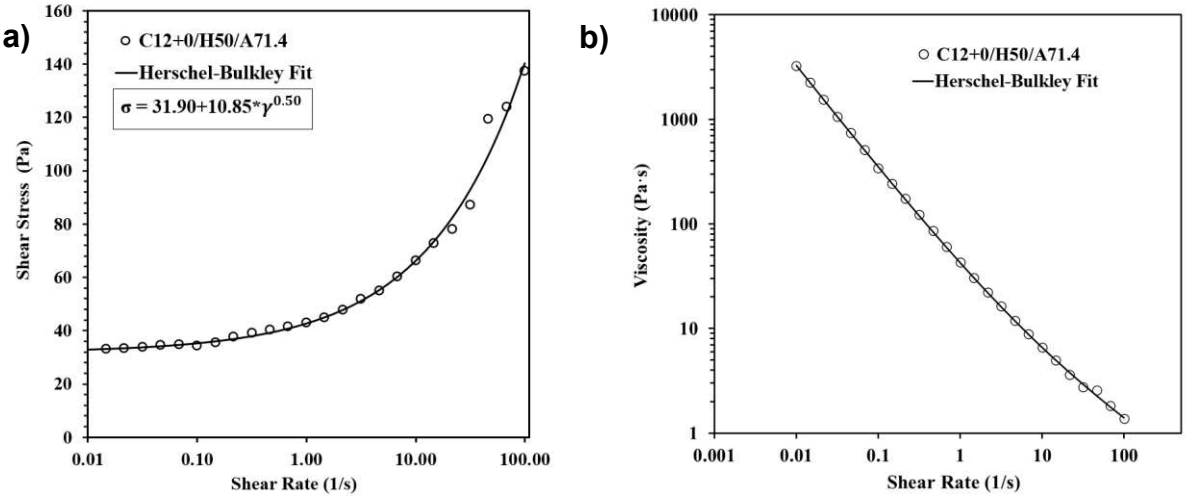

Figure 2. a) Shear stress as a function of shear rate and b) viscosity as a function of shear rate for the fiber foam composition C12+0/H50/A71.4. The solid lines represent the Herschel–Bulkley fit obtained using Eq. (1).

Frequency sweeps

Figure 3 presents frequency sweeps for foams with 12–18 % (w/w) consistency and approximately the same air content. Small variations in air content, however, should be considered when comparing the rheological properties of different foam compositions. The frequency sweep assesses the material response under deformations occurring at different time scales. Low frequencies provide information about material behavior at long time scales, whereas high frequencies represent rapid dynamic deformation. Both storage modulus (G') and loss modulus (G'') increased with increasing fiber consistency as the addition of fibers provides mechanical reinforcement to the foam. Across the examined frequency range, G' increased

monotonically, while G'' remained approximately constant, leading to a decrease in the loss tangent ($\tan \delta = G''/G'$) with increasing frequency (see Figure 3). Based on the classical distinction between viscoelastic liquids and viscoelastic solids, this frequency dependence is consistent with a viscoelastic liquid classification. At the same time, the consistent dominance of G' over G'' indicates that the foam behaves predominantly as an elastic, solid-like material at small deformations within the investigated frequency range. This response is consistent with the presence of a well-structured fiber network. Notice that, in general, the inclusion of additives did not change the frequency dependence of G' and G'' (data not shown).

In paper physics, the fiber suspension connectivity is often estimated by calculating the crowding number N, which is defined as (Kerekes and Schell 1992)

$$N = \frac{\pi c L^2}{6\omega}. \quad (2)$$

Above, c is the fiber mass concentration (kg m^{-3}), L is the average fiber length, and ω is the average coarseness of fibers (kg m^{-1}). Kerekes and Schell (1992) suggested that when $N > 60$, the fibers have at least three contacts and the network becomes rigid. Celzard *et al*. (2009) verified this later by using percolation theory, which describes how a continuous network forms once a critical concentration of elements is reached, changing material properties. At a considerably higher crowding number of approximately 200, Benselfelt et al. (2023) reported a transition to a volume-spanning arrested state (VAS), in which fiber mobility is strongly restricted and the network exhibits solid-like behavior. Notice that for fiber foams the crowding number is obtained by multiplying N with $(1 - \phi_a)$, where ϕ_a is the air volume fraction (Koponen *et al*. 2016).

An equivalent definition for N is (Sellman *et al.* 2024)

$$N = \frac{2}{3} a^2 \phi_f, \quad (3)$$

where a is the fiber aspect ratio and ϕ_f is the fiber volume fraction. Sellman *et al*. (2024) presented phase diagrams of the rheological behavior of fiber suspensions based on the fiber aspect ratio and fiber volume fraction.

For the fiber mixtures used here, the average fiber length and coarseness in Eq. (2) can be calculated with the formulae presented in Koponen *et al*. (2025). The crowding number was N = 211 for the REF/C12/H50/A75.3 fiber foam, which had the highest air content among the samples with the lowest consistency (12% (w/w)). For other fiber foam samples, the crowding number was higher. Thus, all fiber foam samples investigated here can be expected to be in a volume-spanning arrested state, even without accounting for fiber swelling. This interpretation is consistent with the predominantly elastic response observed in the frequency sweeps shown in Figure 3.

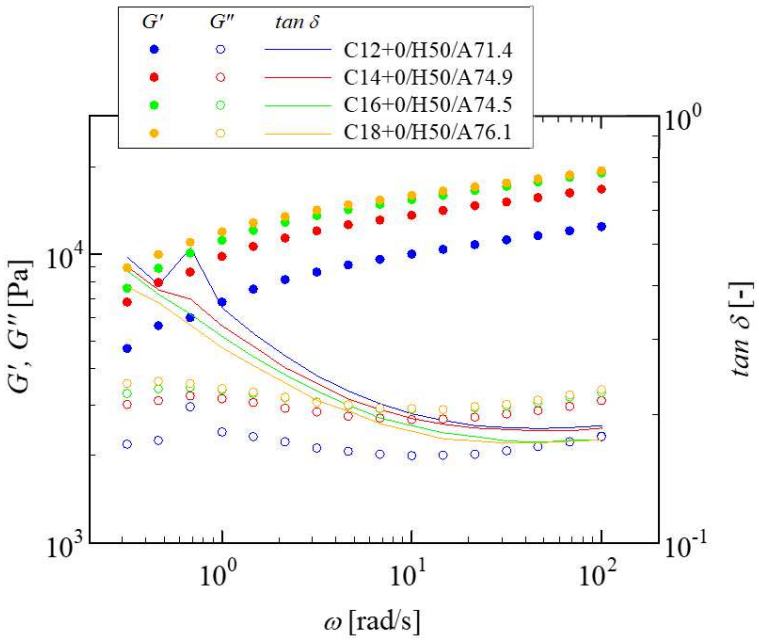

Figure 3. Frequency sweeps for different fiber consistencies.

Amplitude sweeps

Figure 4 shows the corresponding amplitude sweeps for different fiber consistencies at approximately the same air content. We see that at low strain amplitudes G' is significantly higher than G'', indicating a predominantly solid-like behavior. We also see that both G' and G'' increase with increasing fiber consistency. At the flow point, G'' becomes larger than G', marking the transition to flowable, predominantly liquid-like behavior. The flow point occurred at strain amplitudes of approximately 50–150% and tended to shift toward higher strain amplitudes with increasing fiber consistency. The tendency to transition to liquid-like behavior at large deformations makes these foams suitable for applications such as 3D printing, where a fluid-like response is required for flow through the nozzle and a more solid-like behavior at small stresses is needed to prevent unintentional flow through the nozzle when printing is stopped. Similarly, the suitability of high-consistency fiber foams for 3D printing applications is supported by their Herschel–Bulkley type of flow behavior, exhibiting a yield stress and strongly shear-thinning behavior at high shear rates.

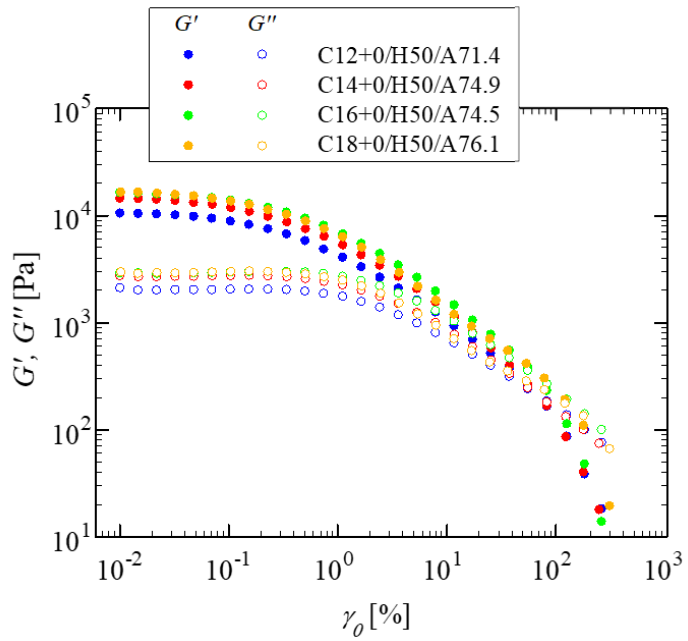

Figure 4. Amplitude sweeps for different fiber consistencies.

We determined the values of the storage and loss moduli in the linear viscoelastic (LVE) region. The LVE region was defined as the strain amplitude range over which G' and G'' remained approximately constant, indicating undisturbed material structure. The onset of nonlinearity was identified as the point where G' or G'' deviated by more than 5% from its initial plateau value (as indicated by ISO 6721-10). The storage and loss moduli representative of the LVE region, G'_{LVE} and G''_{LVE}, were calculated as the averages of G' and G'' within this linear range. Overall, all samples exhibited a strain-sensitive structure indicated by their narrow LVE region for G'. Table 1 shows these values for the different foam compositions.

To compare the stiffness of these high-consistency fiber foams with that of a corresponding pure aqueous foam, the storage modulus of a pure aqueous foam was estimated from the following equation introduced by Saint-Jalmes and Durian (1999):

$$G' = \alpha \frac{\sigma}{R_{32}} \varphi(\varphi - \varphi_c). \qquad (4)$$

Above, α is a numerical pre-factor (=1.4 for 3D disordered polydisperse foams), σ is the surface tension, R_{32} is the Sauter mean radius, φ is the air content, and φ_c is the random close packing volume fraction. For monodisperse foams $\varphi_c = 0.64$, whereas Farr and Groot (2009) report $\varphi_c \approx 0.68$ for polydisperse foams. Corresponding to the fiber foams studied in this paper, we can estimate the surface tension of an air/water interface covered with a 1:1 mixture of SDS and Tween 20 to be 51 mN/m (Muñoz *et al.* 2004) and the Sauter mean radius of air bubbles in fiber foam has been reported to be on the order of 50–100 µm (Hjelt *et al.* 2022; Koponen *et al.* 2020). Assuming a typical air content of 75%, the storage modulus of a pure aqueous foam is estimated to be on the order of 100 Pa. Table 1 shows that the storage modulus of fiber foams at air contents of approximately 75% is on the order of 10^4 Pa. We can therefore conclude that, in the calculated example, the storage modulus of the high-consistency fiber foam is approximately two orders of magnitude greater than that of a fiber-free aqueous foam. This

suggests that the shear stiffness of high-consistency fiber foams originates predominantly from the continuous, three-dimensional fiber network within the foam, while the contribution of the surface energy of the air–water interfaces to the overall foam stiffness is small.

Traditionally, fiber consistency and air content have been considered separately when analyzing fiber foam systems. However, this approach can complicate the interpretation of measurement data, particularly when air content varies between samples. Treating these factors independently may obscure their combined influence on foam structure and properties. To address this, we use fiber volume fraction (FVF), ϕ_f, as a unified parameter that integrates fiber consistency and air content, representing the effective solid phase within the foam matrix. This metric enables a more direct correlation between foam composition and its physical properties. Fiber volume fraction can be calculated using the following equation

$$\phi_f = \frac{m - V\rho_a}{\rho_f V\left(\frac{1}{c} - \frac{\rho_a}{\rho_f} - \frac{\rho_a}{c\rho_w} + \frac{\rho_a}{\rho_w}\right)}. \quad (5)$$

Above, c is fiber mass consistency (w/w), ρ_f = 1500 kg/m^3 is the density of fibers, ρ_w = 1000 kg/m^3 is the density of water, ρ_a = 1.2 kg/m^3 is the density of air, V is the volume of the fiber foam, and m is the mass of the fiber foam. In addition to wood fibers, MCC, PEG and MC were also considered part of the fiber phase.

Notice that wood fibers typically swell in water, but this effect was not addressed due to the difficulty of accurately estimating the degree of swelling. Therefore, ϕ_f should be interpreted as a nominal fiber volume fraction. Table 1 summarizes the fiber volume fractions of different fiber foam samples.

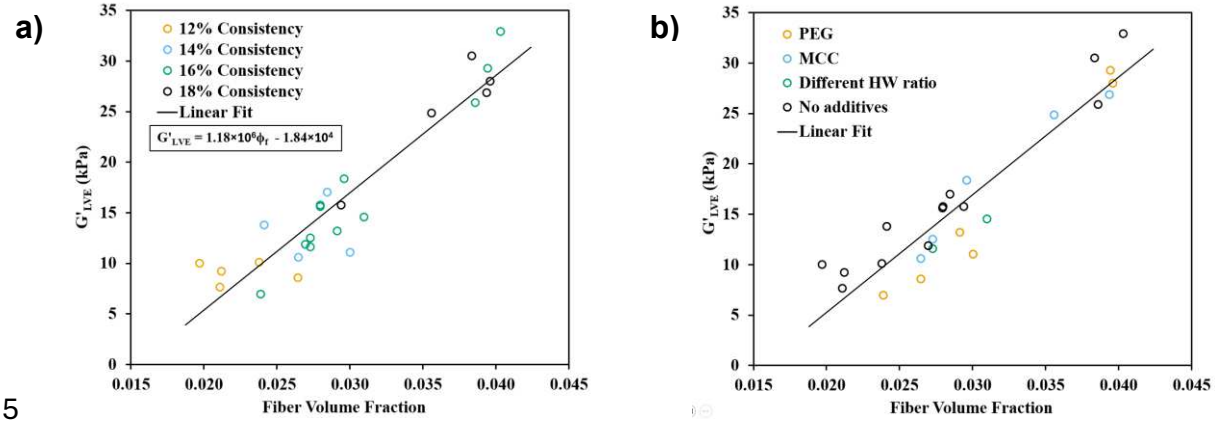

Figure 5. Storage modulus G'_{LVE} as a function of fiber volume fraction ϕ_f: (a) for different fiber consistencies; (b) for different foam compositions. The solid line represents a linear fit to the data points.

Figure 5 shows the storage modulus G'_{LVE} as a function of the fiber volume fraction. The solid line represents a linear fit (R^2 = 0.88) to the data points, with G'_{LVE} given in Pa:

$$G'_{LVE} = 1.18 \times 10^6 \phi_f - 1.84 \times 10^4. \quad (6)$$

Although some scatter is present, the data show that G'_{LVE} generally increases with increasing

fiber volume fraction. As the fiber volume fraction increases, the density of fiber–fiber contacts rises and mechanical constraints become more pronounced, thereby increasing the stiffness of the fiber network. From Figure 5a, we observe that the different consistencies are distributed fairly uniformly on both sides of the fitted line of Eq. (6). In contrast, different foam compositions seem to give slightly different storage moduli. For example, at a given fiber volume fraction, the reference samples without additives exhibited higher storage moduli than the PEG-containing samples. While a linear fit adequately describes the present dataset, comparison with literature data at lower fiber volume fractions suggests that the relationship may become nonlinear across a broader range of fiber volume fractions.

Malm *et al.* (2025) reported data on the relationship between storage modulus and fiber volume fraction over the range $0.007 < \phi_f < 0.03$. They prepared the fiber foams at 20% consistency using unrefined bleached softwood kraft pulp (BSKP) and bleached chemi-thermo-mechanical pulp (CTMP). Simulsol SL10 was used as the surfactant and carboxymethyl cellulose (CMC) was used as an additive. The air content varied between 65–90%. Rheological properties were measured at 25 °C using the same measurement setup as in the present study, with the storage modulus G' determined at a strain amplitude of 0.025% and an angular frequency of 10 rad/s.

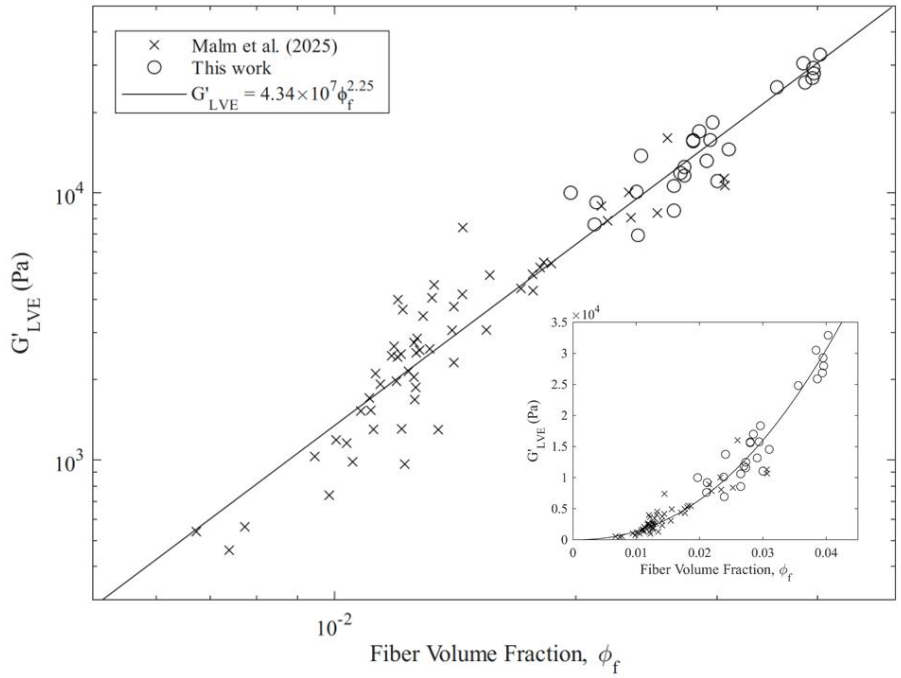

Figure 6. Storage modulus G'_{LVE} as a function of fiber volume fraction. Data extracted from Malm *et al*. (2025) are indicated by ×, and data from this work are shown as ○. The solid line represents a power-law fit given by Eq. (7) to all data points. The inset shows the same data set with linear axes.

Figure 6 shows data from Malm *et al*. (2025) together with data from this work. The two data sets complement each other well and appear to follow a power-law relationship. The solid line in Figure 6 represents a power-law fit to all data points ($R^2 = 0.93$):

$$G'_{\mathrm{LVE}} = 4.34\times10^{7}\,\phi_f^{2.25}. \qquad (7)$$

(Above, G'_{LVE} is given in Pa.) The exponent of 2.25 indicates a strong, nonlinear dependence of the storage modulus on fiber volume fraction, consistent with the presence of a mechanically percolated fiber network, whose stiffness increases nonlinearly with fiber content. Minor deviations from the fit may be attributed to differences in fiber foam composition and dispersion state, and experimental uncertainties.

Assuming that the fiber foams can be treated as relatively isotropic and homogeneous, the storage modulus in the LVE regime can be considered to be proportional to the Young's modulus (Gibson and Ashby 1997). This relationship allows the scaling exponent obtained here (n = 2.25, Eq. 7) to be compared with studies on the density dependence of Young's modulus in dry fiber networks, since the fiber volume fraction is directly proportional to the fiber mass per unit foam volume. The comparison is further supported by the fact that the stiffness of high-consistency fiber foams is governed predominantly by the presence of a continuous, three-dimensional fiber network within the foam, with only a minor contribution from the fluid phase. The exponent $n > 2$ indicates that the network stiffness increases slightly faster than the ideal bending-dominated scaling $n = 2$ predicted for low-density, non-affine fiber networks, where deformation is primarily accommodated by fiber bending (Amjad and Picu 2025; Malekzadeh *et al.* 2021).

The power-law relationship between the fiber volume fraction and the fiber foam stiffness can also be interpreted in light of the tube model and reptation theory, which describe the slow, snake-like movement of long, entangled polymer chains through a virtual "tube" formed by surrounding molecules (De Gennes 1971). Similarly, in high-consistency fiber foams, fiber motion is constrained by the surrounding fibers, and the continuous, three-dimensional fiber network is supported by the bubble matrix. Although the mechanisms differ from those in entangled polymer systems, the resulting confinement provides a useful analogy to the tube model and motivates comparison of the observed scaling behavior with predictions from polymer physics. The tube model predicts that the plateau modulus scales as $G_p \sim \phi^{2.25}$ for semidilute and concentrated entangled polymer solutions (De Gennes 1979). This is identical to the power-law scaling observed for high-consistency fiber foams, $G'_{\mathrm{LVE}} \sim \phi_f^{2.25}$. This correspondence suggests a potentially useful analogy between the dynamics of polymer solutions and high-consistency fiber foams, motivating future studies to test this hypothesis across a broader range of fiber foam systems.

Conclusions

This study provides new insights into the rheological behavior of high-consistency aqueous cellulose fiber foams, with fiber consistencies ranging from 12% to 18% (w/w) and air contents between 63% and 80%. The research demonstrated that these fiber foams exhibit Herschel–Bulkley fluid characteristics, including a yield stress and power-law behavior at high shear rates. In all the studied fiber foam samples, the storage modulus (G') was larger than the loss modulus (G'') at small deformations, indicating a predominantly solid-like, elastic response. This viscoelastic profile is particularly advantageous for applications such as 3D printing, where shape retention is essential. Furthermore, it was concluded that the shear stiffness of

high-consistency fiber foams is dominated by the continuous, three-dimensional fiber network within the foam.

Fiber volume fraction (FVF) was introduced as a unified structural parameter integrating fiber consistency and air content. This approach enables a more direct correlation between foam composition and rheological properties. The storage modulus exhibited a power-law dependence on FVF, similar to the density-dependent scaling of stiffness in rigid fiber networks. The observed scaling exponent was also close to that predicted by the tube model for semidilute entangled polymer solutions. Although this correspondence suggests a possible analogy, the present analysis should be regarded as an initial step toward understanding the underlying mechanisms.

The findings provide a basis for designing and optimizing high-consistency fiber foam processes, with potential relevance to energy-efficient manufacturing and advanced forming applications. Further studies are needed to validate the observed scaling over a broader range of conditions and to determine how fiber dimensions and morphology, bubble size, temperature, surfactant chemistry, additives, and processing history affect fiber-foam rheology.

Acknowledgments

This work was funded by the European Union NextGenerationEU. The project is part of VTT's strategic research initiative "Industrial Energy Efficiency and Low-Carbonisation," launched with support from the additional chapter of the RePowerEU investment and reform programme for sustainable growth in Finland. The authors would like to thank Ari Jäsberg for valuable assistance with the analysis of fiber volume fraction, and Jaakko Asikainen for project management and supervision throughout this work.

Author contributions

D.M.A. developed the fiber-foam formulations, performed the rheological measurements, compiled the experimental data, and contributed to the interpretation of the results, particularly regarding the chemical aspects. O.-V.L. provided training and methodological guidance for the rheological measurements and discussed the progress of the work with D.M.A. J.C.K. coordinated the project, consulted D.M.A. on the fiber-foam formulations, and supported him throughout the study. O.-V.L. and A.K. were primarily responsible for the interpretation of the results. A.K. had primary responsibility for preparing the manuscript, wrote the majority of the text, and guided the writing process. All authors participated in discussions of the results throughout the study. All authors contributed to reviewing and editing the manuscript and approved the final version.

Use of AI-based language models

AI-based language models ChatGPT (OpenAI, San Francisco, CA, USA) and Microsoft Copilot (Microsoft Corporation, Redmond, WA, USA) were used to improve readability and refine language in the manuscript. The AI was not used for data analysis, interpretation or scientific conclusions. The authors take full responsibility for the final content and any errors.

References

Amjad, S.; Picu, R., Strength and stiffness of network materials with preferentially oriented fibers, *Journal of the Mechanics and Physics of Solids* **2025**, *200*, 106101. https://doi.org/10.1016/j.jmps.2025.106101

Barnes, H.; Nguyen, Q., Rotating vane rheometry—a review. *J. Non-Newtonian Fluid Mech.* **2001**, *98*(1), 1–14. https://doi.org/10.1016/S0377-0257(01)00095-7

Benselfelt, T.; Kummer, N.; Nordenström, M.; Fall, A. B.; Nyström, G.; Wågberg, L. The Colloidal Properties of Nanocellulose. *ChemSusChem* **2023**, *16*(8), e202201955. https://doi.org/10.1002/cssc.202201955

Carraretto, I. M.; Owens, C. E.; McKinley, G. H., Time-resolved rheometry of coarsening foams using three-dimensionally printed fractal vanes, *Phys. Fluids* **2022**, *34*(11), 113108. https://doi.org/10.1063/5.0119944

Celzard, A.; Fierro, V.; Kerekes, R., Flocculation of cellulose fibres: New comparison of crowding factor with percolation and effective-medium theories, *Cellulose* **2009**, *16*(6), 983–987. https://doi.org/10.1007/s10570-009-9314-0

Chaparian, E.; Owens, C.; McKinley, G., Computational rheometry of yielding and viscoplastic flow in vane-and-cup rheometer fixtures, *J. Non-Newtonian Fluid Mech.* **2022**, *307*, 104857. https://doi.org/10.1016/j.jnnfm.2022.104857

Coughlin, M.; Liberman, L.; Ertem, S.; Edmund, J.; Bates, F.; Lodge, T., Methyl cellulose solutions and gels: fibril formation and gelation properties, *Prog. Polym. Sci.* **2021**, *112*, 101324. https://doi.org/10.1016/j.progpolymsci.2020.101324

Crawford, N.; Sprague, M.; Stickel, J., Mixing behavior of a model cellulosic biomass slurry during settling and resuspension, *Chem. Eng. Sci.* **2016**, *144*, 310–320. https://doi.org/10.1016/j.ces.2016.01.028

De Gennes, P. G., Reptation of a polymer chain in the presence of fixed obstacles, *J. Chem. Phys.* **1971**, *55*(2), 572–579. https://doi.org/10.1063/1.1675789

De Gennes, P. G., Scaling concepts in polymer physics. Cornell University Press, 1979.

Dollet, B.; Raufaste, C., Rheology of foams, *Comptes Rendus. Physique* **2014**, *15*(8–9), 731–747. https://doi.org/10.1016/j.crhy.2014.09.008

Farr, R.; Groot, R., Close packing density of polydisperse hard spheres, *J. Chem. Phys.* **2009**, *131*(24), 244104. https://doi.org/10.1063/1.3276799

Gibson, L.; Ashby, M., Cellular solids: structure and properties. Cambridge University Press, Cambridge, 1997.

Hafez, I.; Tajvidi, M., Comprehensive insight into foams made of thermomechanical pulp fibers and cellulose nanofibrils via microwave radiation, *ACS Sustain. Chem. Eng.* **2021**, *9*(30), 10113–10122. https://doi.org/10.1021/acssuschemeng.1c01816

Hjelt, T.; Ketoja, J.; Kiiskinen, H.; Koponen, A.; Pääkkönen, E., Foam forming of fiber products: a review, *J. Dispersion Sci. Technol.* **2022**, *43*(10), 1462–1497. https://doi.org/10.1080/01932691.2020.1869035

Jäsberg, A.; Selenius, P.; Koponen, A., Experimental results on the flow rheology of fiber-laden aqueous foams. *Colloids Surf. A* **2015**, *473*, 147–155. https://doi.org/10.1016/j.colsurfa.2014.11.041

Jäsberg, A.; Selenius, P.; Koponen, A., The effect of fibrous materials on the rheology of aqueous foams. In *Proceedings of the 16th Fundamental Research Symposium*, Robinson Pembroke College, Oxford, UK, 3–8 September 2017; pp 159–174. https://doi.org/10.15376/frc.2017.1.159

Kerekes, R.; Schell, C., Characterization of fiber flocculation regimes by a crowding factor. *J Pulp Paper Sci* **1992**, *18*, J32–J38.

Ketola, A.; Song, W.; Lappalainen, T.; Salminen, K.; Viitala, J.; Turpeinen, T.; Miettinen, A.; Lee, K.-Y.; Ketoja, J., Changing the structural and mechanical anisotropy of foam-formed cellulose materials by affecting bubble–fiber interaction with surfactant, *ACS Appl. Polym. Mater.* **2022a**, *4*(10), 7685–7698. https://doi.org/10.1021/acsapm.2c01248

Ketola, A.; Hjelt, T.; Lappalainen, T.; Pajari, H.; Tammelin, T.; Salminen, K.; Lee, K.; Rojas, O.; Ketoja, J., The relation between bubble-fibre interaction and material properties in foam forming. In *Advances in Pulp and Paper Research*, Cambridge 2022, Trans. of the XVIIth Fund. Res. Symp.; Coffin, D., Batchelor, W., Eds.; FRC: Manchester, 2022b; pp 65–84. https://doi.org/10.15376/frc.2022.1.65

Koponen, A.; Kiiskinen, T.; Pääkkönen, E., Effect of fibre properties on the structure, strength, and thermal conductivity of foam-formed and air-laid cellulosic lightweight fibrous materials, *BioResources* **2025**, *20*(4), 10922–10958. https://doi.org/10.15376/biores.20.4.10922-10958

Koponen, A.; Timofeev, O.; Jäsberg, A.; Kiiskinen, H., Drainage of high-consistency fiber-laden foams, *Cellulose* **2020**, *27*(15), 9637–9652. https://doi.org/10.1007/s10570-020-03416-y

Koponen, A.; Torvinen, K.; Jäsberg, A.; Kiiskinen, H., Foam forming of long fibers, *Nordic Pulp & Paper Research Journal* **2016**, *31*(2), 239–247, https://doi.org/10.3183/NPPRJ-2016-31-02-p239-247

Lehmonen, J.; Retulainen, E.; Paltakari, J.; Kinnunen-Raudaskoski, K.; Koponen, A., Dewatering of foam-laid structures and formed web properties. *Cellulose* **2020**, *27*(3), 1127–1146. https://doi.org/10.1007/s10570-019-02842-x

Li, Y.; Xie, M.; Liu, Y.; Zhao, H., Influence of fiber aspect ratio and CPAM on bubble dynamics and rheology in bagasse suspensions. *ACS Omega* **2025**, *10*(33), 37617–37627. https://doi.org/10.1021/acsomega.5c04010

Malekzadeh, H.; Md Zaid, N.; Bele, E., Characterization and structural properties of bamboo fibre solid foams. *Cellulose* **2021**, 28, 703–714. https://doi.org/10.1007/s10570-020-03565-0

Malm, T.; Rokkonen, T.; Minkkinen, H.; *et al*., Method for Manufacturing a Fiber-Based Industrial Material, Fiber-Based Industrial Material and Apparatus for Manufacturing a Fiber-Based Industrial Material, WO2025119466A1, 2025.

Miranda-Valdez, I.; Yazdani, M.; Mäkinen, T.; Coffeng, S.; Viitanen, L.; Koivisto, J.; Alava, M., Cellulose foams as scalable templates for phase change materials. *J. Energy Storage* **2023**, *73*, 109036. https://doi.org/10.1016/j.est.2023.109036

Mohtaschemi, M.; Dimic-Misic, K.; Puisto, A.; Korhonen, M.; Maloney, T.; Paltakari, J.; Alava, M., Rheological characterization of fibrillated cellulose suspensions via bucket vane viscometer, *Cellulose* **2014**, *21*, 1305–1312. https://doi.org/10.1007/s10570-014-0235-1

Muñoz, M.; Rodríguez, A.; Graciani, M. D. M.; Moyá, M. L., Conductometric, Surface Tension, and Kinetic Studies in Mixed SDS−Tween 20 and SDS− SB3-12 Micellar Solutions, *Langmuir* **2004**, *20*(*25*), 10858−10867. https://doi.org/10.1021/la048247n

Nasatto, P.; Pignon, F.; Silveira, J.; Duarte, M.; Noseda, M.; Rinaudo, M., Methylcellulose, a cellulose derivative with original physical properties and extended applications, *Polymers* **2015**, *7*(5), 777–803. https://doi.org/10.3390/polym7050777

Prakash, B.; Jäsberg, A.; Koponen, A., Experimental investigation on the effect of fibre consistency on rheology of aqueous foams in pipe flow, *Annu. Trans. Nord. Soc. Rheol.* **2021**, *29*, 27–34.

Saint-Jalmes, A.; Durian, D. J., Vanishing elasticity for wet foams: Equivalence with emulsions and role of polydispersity, *J. Rheol.* **1999**, *43*(*6*), 1411−1422. https://doi.org/10.1122/1.551052

Sellman, F.; Rostami, J.; Östmans, R.; *et al.*, Influence of fibril aspect ratio, chemical functionality, and volume fraction on the mechanical properties of cellulose nanofibril materials, *Cellulose* **2024**, *31*, 8007–8025. https://doi.org/10.1007/s10570-024-06084-4

Vadillo, D. C.; Owens, C. E.; Perego, A.; McKinley, G. H. Vane rheometry of viscoelastic liquids and yield stress fluids. *Rheologica Acta* **2025**, 64(6–7), 315–335. https://doi.org/10.1007/s00397-025-01498-8